Radio Science, Volume 35, Number 5, Pages 1129–1141, September–October 2000

A simulation study of coherent radar imaging

Tian-You Yu and Robert D. Palmer

Department of Electrical Engineering and Center for Electro-Optics
University of Nebraska, Lincoln

David L. Hysell

Department of Physics and Astronomy, Clemson University, Clemson, South Carolina

Abstract. Coherent radar imaging (CRI) is used in an attempt to overcome the angular resolution limitation of conventional single-station radars and is used to image the horizontal structure inside the resolution volume. This recently developed technique has been successfully applied to radar observations of the ionosphere as well as the lower atmosphere. However, no statistical analysis of the robustness of the various techniques has been presented to date. In this work, three CRI techniques are reviewed: Fourier-based, Capon's, and maximum entropy (MaxEnt) methods. The Fourier-based method is the simplest of the three algorithms but has inherent resolution limitations. Although quite different in nature and performance, both Capon's and MaxEnt methods can be posed as constrained optimization problems. A statistical comparison of performance of the three CRI techniques, using various receiver configurations and two distinct cases of scattering structure, is made using simulated data. The results show that the MaxEnt method exhibits the best performance in the case of aspect-sensitive scattering with a broad characteristic. In the localized scattering case, however, Capon's method shows superior performance for signals with high signal-to-noise ratio (SNR), but MaxEnt method outperforms all methods for low SNR. In general, both Capon's and MaxEnt methods are able to reproduce the gross characteristics of the scattering media under observation.

1. Introduction

Coherent radar imaging (CRI), an outgrowth of radar interferometry [*Woodman*, 1971], has the potential to reveal the evolution of the structure of scattering media inside the resolution volume. Moreover, making use of its Doppler sorting property, an additional dimension of velocity is possible. With the knowledge of how the atmospheric structure evolves both in time and space within the radar beam, which is provided by CRI, ambiguities between spatial and temporal dimensions which arise from single station radar observations can be mitigated. Various algorithms of CRI such as Fourier-based, MaxEnt, and Capon's methods have been successfully applied to atmospheric observations [e.g., *Kudeki and Sürücü*, 1991; *Hysell*, 1996; *Palmer et al.*, 1998a], but no statistical comparisons of performance among these algorithms has been made. The present work is an attempt to validate and quantify the performance of the various algorithms of CRI.

One manner in which to interpret CRI is from the beam-forming point of view. A synthesized beam, pointing at one specific direction, can be formed by the introduction of an appropriate weighting function onto the signals from the spatially separated receivers. By steering this beam by the modification of the weighting function the so-called brightness distribution within the transmitter beam can be estimated. The brightness distribution is a term which refers to the averaged signal power density as a function of angle and Doppler shift [e.g, *Thompson*, 1986]. With this beam-forming viewpoint it can be seen that the resolution of the estimated brightness distribution is dictated by the pattern of the synthesized beam which is determined by the receiver

Paper number 1999RS002236.
0048-6604/00/1999RS002236$11.00

configuration and weighting function. Higher resolution can be achieved more economically by lengthening the distance between receivers as well as increasing the number of receivers rather than by increasing the aperture of the main array of a conventional radar system. Furthermore, sophisticated signal-processing techniques can be used to provide improved resolution for a given receiver configuration. For example, the MaxEnt and Capon's methods can produce higher resolution and more statistically robust images than the conventional Fourier-based method [e.g., *Hysell*, 1996; *Hysell and Woodman*, 1997; *Palmer et al.*, 1998a].

The first application of CRI was made by *Kudeki and Sürücü* [1991] for the observation of field-aligned plasma irregularities in the equatorial electrojet using the Jicamarca radar. The brightness distribution was estimated by taking the discrete Fourier transform of windowed visibility spectrum (normalized cross-spectrum) estimated using signals from spatially separated receiver pairs. A rectangular window function was applied to the received signals, resulting in a sinc-shaped synthesized beam pattern limiting the resolution of the images [*Kudeki and Sürücü*, 1991]. As a result, *Hysell* [1996] applied the maximum entropy (MaxEnt) algorithm to data from the Jicamarca radar and produced resolution-enhanced images of F region irregularities. Entropy has applications in information theory and can be interpreted as the averaged information content of the brightness distribution [*Shannon and Weaver*, 1949]. By maximizing the entropy of the brightness distribution the MaxEnt method produces an image which is the most consistent with the available observed data [*Thompson*, 1986]. A general review of CRI has been given by *Woodman* [1997], who provided the linear relationship between visibility and brightness distribution. It was further shown that this equation could be solved only in special cases.

The pioneering CRI work in the ionosphere focused on imaging one-dimensional field-aligned structures using linear receiving arrays. The first two-dimensional estimates of the brightness distribution were shown by *Palmer et al.* [1998a]. In their paper, a two-dimensional generalization of CRI was derived, and another resolution-enhanced technique, Capon's method [*Capon*, 1969], was applied to the CRI problem. Capon's method is an adaptive technique which has the capability of suppressing interfering signals and also results in an increased resolution. The interfering signals are signals originating from directions other than the direction where the brightness distribution is estimated. By applying Capon's method to data obtained using the middle and upper (MU) atmosphere radar in Shigaraki, Japan, during the Baiu season, *Palmer et al.* [1998a] produced high-resolution two-dimensional images of the lower atmosphere. In addition, the Doppler sorting capability of CRI was used to generate a set of brightness distribution estimates due to precipitation particles of various fall velocities during stratiform precipitation.

A brief review of Fourier-based, Capon's, and MaxEnt methods is presented in section 2. The goal of this work is to validate the use of CRI through simulations where the governing atmospheric parameters are known and controllable. Thus a physical simulation model which was described by *Holdsworth and Reid* [1995] and *Holdsworth* [1995] was used for the results provided in section 3. Two cases, broad, aspect-sensitive scattering and localized scattering regions, were simulated and used to test the capability of the three CRI techniques. The effects of additive noise and receiver configuration on the estimation of the brightness distribution were quantified. By calculating the peak of the normalized cross correlation between the model brightness distribution and those produced by the CRI techniques a quantitative performance comparison of the Fourier-based, Capon's, and MaxEnt methods will be presented.

2. Review of Coherent Radar-Imaging Techniques

2.1. General Description

The CRI problem can be posed as an attempt to estimate the brightness distribution given a finite number of spatial samples which are made using spatially separated receivers [*Woodman*, 1997]. Because of the random nature of these signals from spaced receivers a statistical description is needed. Therefore the visibility function is used, which is the spatial correlation function of the received signals. If the continuous form of visibility function is known, which in general requires an infinite number of receivers, the brightness distribution can be obtained by performing the spatial Fourier transform of the visibility function [e.g., *Thompson*, 1986]. In practice, only a finite number of receivers are available, resulting in a visibility function defined only at certain spatial lags. These lags are defined by the vec-

tors between all combinations of receivers and are termed baselines. If the number of distinct baselines or spatial lags at a given length and angle is larger than 1, it is considered redundant. Specifically, given signals from n receivers, the maximum number of nonredundant baselines is $n(n-1)/2$.

Because the visibility function and brightness distribution are Fourier transform pairs, an intuitive estimate of the brightness distribution is given by the inverse Fourier transform of the available visibility samples. The estimated brightness distribution is the convolution of the true brightness distribution with an angular window function. Therefore the resolution of the estimated brightness distribution is limited by the window function. The resolution can be enhanced by using a priori knowledge of the brightness distribution through a modeling approach [*Woodman*, 1997]. Although many algorithms exist, the present work will compare only the MaxEnt, Capon, and Fourier-based methods. The MaxEnt and Capon methods have recently gained favor in the atmospheric science community because of their high resolution capability. Interestingly, both methods can be formulated as constrained optimization problems. In the MaxEnt case, the algorithm is derived by maximizing the entropy of the brightness distribution on the basis of several constraints such as the integrated brightness distribution and errors in the visibility data. For Capon's method an estimate of the brightness distribution is obtained by minimizing the overall brightness while requiring unity amplitude in the direction where the brightness estimate is made. A brief summary of the methods is provided in sections 2.2-2.4.

2.2. Fourier-Based CRI

Let $\mathbf{D}_1, \mathbf{D}_2, \ldots, \mathbf{D}_n$ represent the position vectors of the n receivers with respect to the origin. Given signals from these n receivers, the visibility matrix $\mathbf{V}$ can be defined in following form:

$$\mathbf{V} = \begin{bmatrix} V_{11}(f) & V_{12}(f) & \ldots & V_{1n}(f) \\ V_{21}(f) & V_{22}(f) & \ldots & V_{2n}(f) \\ \vdots & \vdots & \ddots & \vdots \\ V_{n1}(f) & V_{n2}(f) & \ldots & V_{nn}(f) \end{bmatrix}, \quad (1)$$

where $V_{ij}(f)$ indicates a sample of the visibility function at a spatial lag which is defined by the position vectors of receivers i and j as $\mathbf{D}_i - \mathbf{D}_j$. The temporal frequency is denoted by f. By premultiplying and postmultiplying $\mathbf{V}$ by a weight vector $\mathbf{w}_f$ an estimate of the brightness distribution can be obtained [*Palmer et al.*, 1998a].

$$\hat{B}_f(\mathbf{k}, f) = \mathbf{w}_f^H \mathbf{V} \mathbf{w}_f, \quad (2)$$

where H denotes the Hermitian operator and $\mathbf{k}$ is the wavenumber vector which points toward the direction where the brightness distribution is estimated. In addition, this wavenumber vector is represented by $\mathbf{k} = 2\pi/\lambda \left[\sin\theta\sin\phi \quad \sin\theta\cos\phi \quad \cos\theta \right]$, where λ denotes the radar wavelength and θ and ϕ are the zenith and azimuth angles, respectively. The weight vector has the following form:

$$\mathbf{w}_f = \left[e^{j\mathbf{k}\cdot\mathbf{D}_1} \quad e^{j\mathbf{k}\cdot\mathbf{D}_2} \quad \ldots \quad e^{j\mathbf{k}\cdot\mathbf{D}_n} \right]^T, \quad (3)$$

where T is the transpose operator. From the beamforming point of view, (3) results in a synthesized beam which can be "steered" by introducing proper phase shifts. The shape of this synthesized beam determines the resolution of the brightness distribution estimate and only depends on the locations of receivers. For example, if a linear uniformly spaced receiving array is considered, (3) represents equal weighting on the n received signals, which results in a triangular weighting of the visibility data. Thus a sinc squared synthesized beam is obtained by calculating the spatial frequency response of this triangular weighting function.

2.3. Capon's CRI

As mentioned in section 2.2, the resolution of the Fourier-based method is limited by the width of synthesized beam pattern, which is independent of the pointing direction and the data. *Capon* [1969] proposed a weighting function which adapts to the data and pointing direction in order to achieve superior performance, exemplified by suppression of interference and improved resolution. In other words, by incorporating the information of the data into the weighting function the resulting synthesized beam can null interference automatically. Without the contamination of interference the resolution is expected to be improved. Mathematically, Capon's method can be posed as a constrained optimization problem. By minimizing the overall brightness with respect to the weight vector, incoming signals (including interfering signals) should be suppressed. However, the minimization is constrained such that

the frequency response of the weight vector is unity in the direction where the brightness is estimated. A complete derivation and further discussion are given by *Palmer et al.* [1998a]. This constrained optimization problem can be solved by Lagrange methods resulting in the following form of the weight vector and estimated brightness distribution:

$$\mathbf{w}_c = \frac{\mathbf{V}^{-1}\mathbf{e}}{\mathbf{e}^H\mathbf{V}^{-1}\mathbf{e}}, \tag{4}$$

$$\hat{B}_c(\mathbf{k}, f) = \frac{1}{\mathbf{e}^H\mathbf{V}^{-1}\mathbf{e}}, \tag{5}$$

$$\mathbf{e} = \left[\; e^{j\mathbf{k}\cdot\mathbf{D}_1} \quad e^{j\mathbf{k}\cdot\mathbf{D}_2} \quad \ldots \quad e^{j\mathbf{k}\cdot\mathbf{D}_n} \; \right]^T. \tag{6}$$

Note that the resulting weight vector $\mathbf{w}_c$ is dependent on the data, through the visibility matrix $\mathbf{V}$, and is therefore a truly adaptive technique. In other words, the weights used in the estimation of the brightness distribution for a particular direction change with each additional data set. This is not the case for the Fourier-based method (2) where the weights are fixed for a given direction.

2.4. Maximum Entropy CRI

As pointed out in section 2.2, the visibility function can only be estimated at certain spatial lags because of the finite number of receivers. In the Fourier-based method no prior knowledge is used, and the visibility function at lags where no estimates are made is simply assumed to be zero. However, no such assumption is made in the MaxEnt method. Instead, a model of the brightness distribution is derived, based on constraints and a priori knowledge of a nonnegative brightness. This model, in some sense, can be used to interpolate and extrapolate the visibility function. Therefore a more reliable and higher-resolution image can be obtained. By maximizing the entropy of the model the resulting map is the one most representative of all possible maps, the one most likely to be the true brightness distribution, and the most consistent with the available noisy visibility data. In other words, instead of finding the exact brightness distribution a map of the brightness distribution, which is allowed to deviate from the true map as far as the constraints are satisfied and which has maximum entropy, is found using the MaxEnt method. The entropy $\mathcal{S}$ can be defined as

$$\mathcal{S} = \sum_{\mathbf{k}} B(\mathbf{k}, f) \; \ln B(\mathbf{k}, f)/F, \tag{7}$$

where F is the summation of the brightness distribution over the region of interest.

$$F = \sum_{\mathbf{k}} B(\mathbf{k}, f). \tag{8}$$

The MaxEnt solution can be solved using Lagrange methods by maximizing (7) subject to proper constraints. One constraint imposed is associated with the statistical errors of the visibility data. Let e_j represent the statistical error of the jth visibility sample. The error is assumed to be a Gaussian-distributed random variable with standard deviation σ_j. As a result, the summation of the ratio ${e_j}^2/{\sigma_j}^2$ over M samples has a χ^2 distribution with M degrees of freedom [*Gull and Daniell*, 1978]. M is the number of lags of the visibility function and is calculated as twice the number of nonredundant baselines plus 1. In addition, constraining each noisy visibility datum to be equal to the inverse Fourier transform of the brightness distribution, and constraining the total brightness to a fixed value, as given in (8), the following form of the brightness distribution can be obtained [*Hysell*, 1996; *Hysell and Woodman*, 1997]:

$$\hat{B}_m(\mathbf{k}, f) = Z^{-1} F e^{-\sum_j \lambda_j h_j(\mathbf{k})}, \tag{9}$$

$$Z = \sum_{\mathbf{k}} e^{-\sum_j \lambda_j h_j(\mathbf{k})}, \tag{10}$$

where the so-called point spread function is given by

$$h_j(\mathbf{k}) = \cos / \sin(\mathbf{k} \cdot \Delta\mathbf{D}_j) \tag{11}$$

and is either a cos or sin function depending on whether the real or imaginary part of visibility data is used for the estimation. In addition, $\Delta\mathbf{D}_j$ refers to the baseline of the jth visibility data. The summation j is over M, and $\mathbf{k}$ spans the region where the brightness distribution is to be estimated. By solving the resulting nonlinear set of equations the Lagrange multipliers λ_j can be obtained, providing the estimate of the brightness distribution [*Hysell*, 1996].

3. Simulation Results

3.1. Simulated Radar Configurations

The modeling scheme used for this work was originally designed for both spaced antenna and Doppler radar simulations and has been shown to be ex-

Table 1. List of Simulation Parameters

Parameter	Value
Radar frequency	46.5 MHz
Range	10 km
Range resolution	150 m
Transmitter half-power beam width	3.6°
Transmitter pointing direction	vertical
Receiver beam width	∞
Sampling time	0.1 s
Number of scatterers	200
Horizontal wind magnitude	30 m s^{-1}
Azimuth angle	90°
Vertical wind	0 m s^{-1}
Turbulent rms velocity	0.5 m s^{-1}

tremely flexible for both MF and VHF wavelengths [*Holdsworth and Reid*, 1995; *Holdsworth*, 1995]. The simulation is initiated by randomly positioning a number of scatterers inside the so-called enclosing volume. At each sampling time the complex received signal is obtained by the coherent summation of all returned signals from scatterers inside the enclosing volume. The amplitude of each scatterer's signal depends on a random reflectivity, antenna beam pattern, aspect sensitivity function, and range weighting function. The phase of each scatterer's signal depends on the two-way path from the transmitter to the scatterer and back to the receiver. As time evolves, the positions of the scatterers are updated by a mean wind and a spatially correlated turbulent motion. When a scatterer moves outside the enclosing volume, it is readmitted into the volume as a new scatterer at the opposite location in order to maintain a constant number of scatterers. After the time series data are generated, an appropriately scaled, complex, white, Gaussian noise sequence can be added in order to obtain a noise-corrupted signal with desired SNR. It has been pointed out by *Holdsworth and Reid* [1995] that simplifications, such as assuming a single receiving antenna position and the fact that each data point represents the coherently averaged data, have been tested and do not have significant effects on the results.

For this work, a VHF (46.5 MHz) radar spaced antenna system has been simulated. The parameters used in the simulation are shown in Table 1. The enclosing volume with 200 scatterers was centered at an altitude of 10 km. Scatterers were allowed to advect through the enclosing volume with a horizontal wind magnitude of 30 m s^{-1} with azimuth angle of 90° . No vertical motion was allowed except for that caused by the turbulent motion with a root-mean-square (rms) velocity of 0.5 m s^{-1}. A 1 μs transmitted pulse was used with a Gaussian-shaped range weighting function. The sampling time, including all coherent integration, was set at 0.1 s, and each record of 256 time series points was generated simultaneously for the seven receivers shown in Figure 1c. By taking various combinations of receivers the impact of receiver configuration on the brightness estimates can be studied. Three receiver configurations and corresponding spatial lags where the visibility data are available are shown in Figures 1 and 2, respectively. As indicated in Figure 1a, configuration 1 consists of the center receiver and the three receivers which have shorter radial distances from the center. The outlying receivers are located 19.6 m from the center with azimuth angles of 96.58°, 216.58°, and 336.58°. Configuration 2 has a similar structure to configuration 1, but the outer three receivers are displaced 39.2 m from the origin, and the azimuth angles are shifted 60° counterclockwise with respect to configuration 1. Configuration 3 allows the maximum number of spatial samples of the visibility function by using all seven receivers.

Before examining any CRI-generated brightness

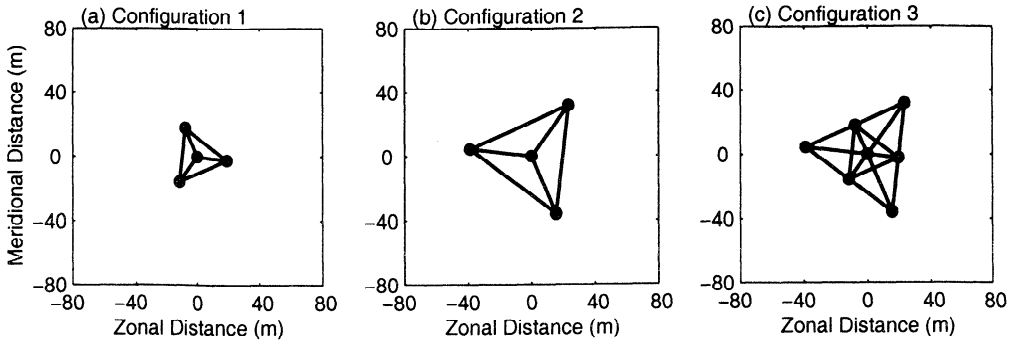

Figure 1. As an initial step in the simulation, the returned signals of the seven receivers shown in Figure 1c are generated simultaneously. The other configurations can be taken as subsets of the original data. Configuration 1 (Figure 1a) has only four receivers with relatively short baseline lengths. With the same basic arrangement, Configuration 2 (Figure 1b) also has four receivers but with longer baseline lengths. Presumably, configuration 3 (Figure 1c) will provide the benefits of both other arrangements.

estimates it is prudent to investigate the grating lobe patterns of the three configurations. These patterns are provided in Figure 3 and illustrate the power pattern of the synthesized beams in the angular domain for the Fourier-based method. The resolution of the Fourier-based method can be characterized by the width of the mainlobe at the center of the images. As expected, the resolution is enhanced by using configuration 2 where the baseline lengths have been increased. However, the grating lobes and sidelobes are closer toward the center and may possibly produce angular aliasing and degrade the reliability of the brightness estimates. In configuration 3, more nonredundant spatial visibility samples are available for the estimation of the brightness distribution. Thus configuration 3 should produce the most statistically robust estimates of the brightness distribution since resolution is relatively high with minimized aliasing. It should be pointed out that a general grating lobe pattern for a given configuration is not available for either Capon's or MaxEnt methods since both techniques depend on the particular data set. However,

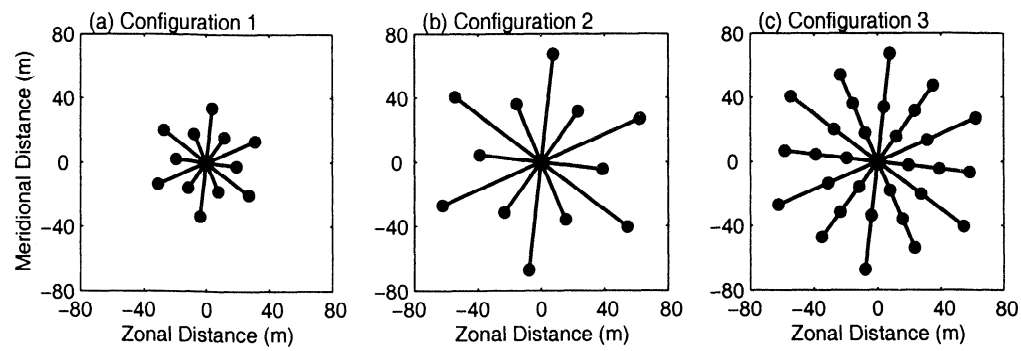

Figure 2. Because a finite number of receivers were used, the visibility function can only be estimated at a limited number of spatial lags, which are denoted by the dots in the plots: (a) configuration 1, (b) configuration 2, and (c) configuration 3. Those spatial lags are calculated by taking a vector difference between any two receivers' position vectors. Configuration 3 has the maximum number of visibility samples and should provide the most reliable estimates of the brightness distribution.

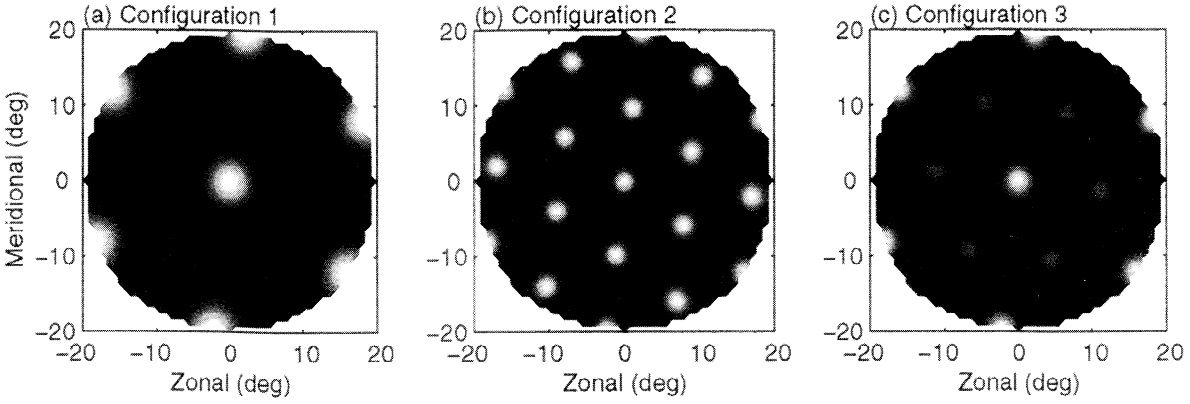

Figure 3. The Fourier grating lobe patterns for (a) configuration 1, (b) configuration 2, and (c) configuration 3 are shown in the figure within 20° of zenith. The white portion of the plots indicates a higher value. When the baseline length increases, the sidelobe effects become more significant in the region of interest, which is approximately within 5° of zenith. In contrast, configuration 3 has the same grating lobe pattern as configuration 1 but with a more narrow mainlobe.

it is still expected that configuration 3 will produce statistically more significant results for both Capon's and MaxEnt methods, because it combines all available visibility data.

Angular variation in the model brightness distribution was simulated by the multiplication of transmit beam pattern and an aspect sensitivity function with desired form. Sections 3.2-3.3 detail the capabilities of the CRI techniques to estimate the brightness distribution for two distinct cases. The first is a broad, slightly horizontally anisotropic pattern indicative of tropospheric or stratospheric scatter. The second aspect sensitivity pattern exhibits two distinct peaks and will provide a qualitative measure of the resolution capabilities of the techniques.

3.2. Case 1: Aspect-Sensitive Scattering

VHF backscattered signals from the neutral atmosphere have been shown to be aspect sensitive, which is manifested by a decrease in echo power as the radar beam points away from zenith [e.g, *Gage and Green*, 1978; *Röttger and Liu*, 1978; *Fukao et al.*, 1979]. Recently, *Palmer et al.* [1998b] showed that the peak of the aspect sensitivity function can be tilted away from zenith as much as 1°. In an attempt to reproduce a realistic situation an aspect sensitivity function, with a meridional elongation, centered at (0.5°, 0.5°), was simulated. The first column of Figure 4 is the modeled brightness distribution and the other three columns are the estimates of the brightness distribution for SNR = 20 dB using Fourier-based, Capon's, and MaxEnt CRI, respectively. In order to obtain reasonable visibility estimates, five records of data (~2 min) were incoherently averaged. As suggested by *Hysell* [1996], the background noise was subtracted from the visibility estimates for the MaxEnt case in order to avoid the solution from reverting to the Fourier-based method. The noise was removed using a polynomial interpolation of the autocorrelation function about zero lag. In limited cases, however, this noise removal procedure was observed to cause the visibility matrix to become singular. As a result, Capon's method did not produce reliable images. In order to compare the best performance of each technique the visibility data without noise subtraction were used in Capon's method, and those with noise subtraction were used in the MaxEnt and Fourier-based methods. In addition, the temporal frequency (f) dependence of the brightness distribution was eliminated through an average over all frequencies. However, this Doppler sorting capability is extremely important and has potential for studies of multiple structures moving with different velocities and for high-resolution maps of radial velocity.

The receiver configuration effect is evident by examining the brightness estimates generated by the Fourier-based method, which is shown in the second column of Figure 4. Notice the severe sidelobe effects

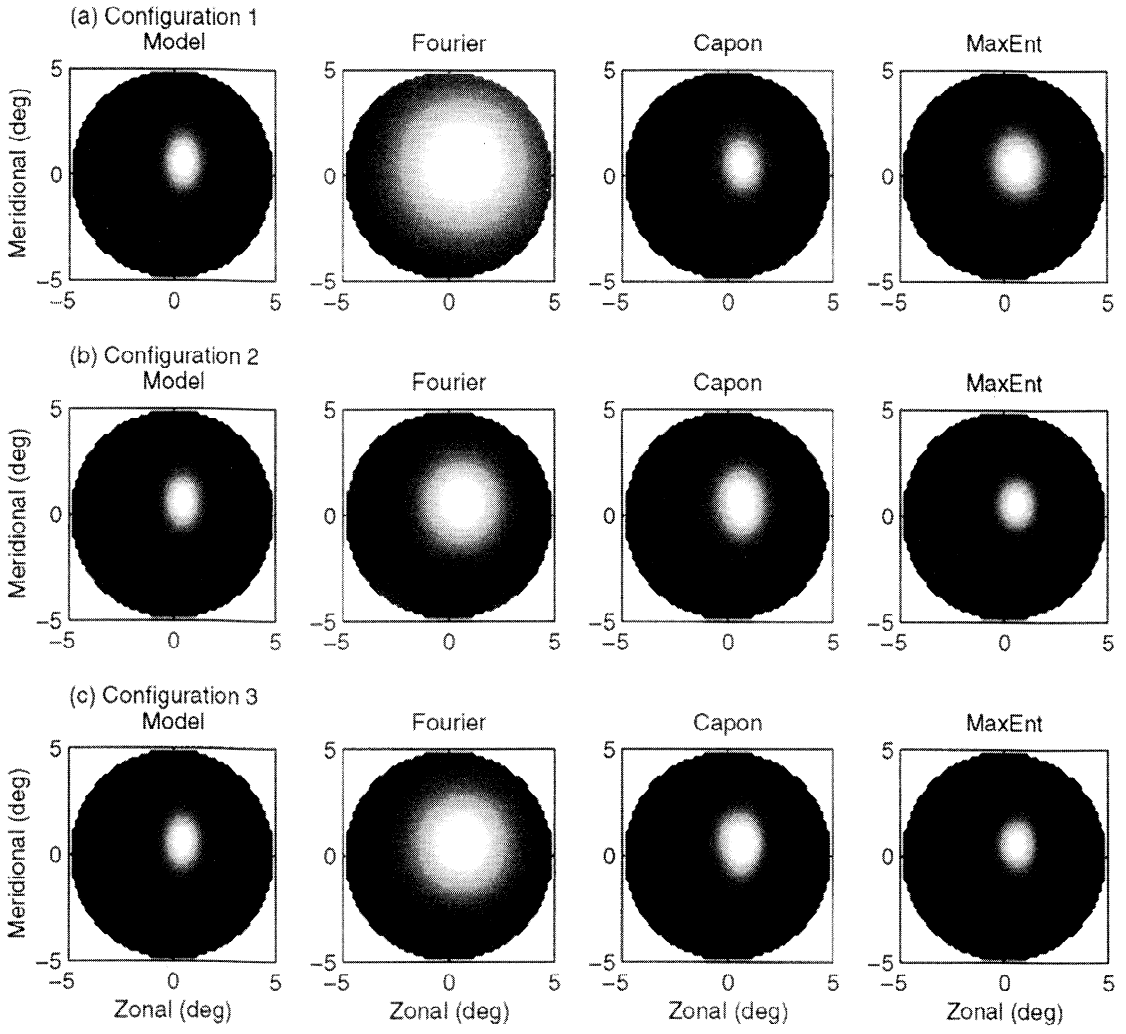

Figure 4. This case depicts a broad aspect-sensitive scattering case which is slightly offset from zenith. Results from the three configurations are shown in Figures 4a, 4b, and 4c. The brightness estimates for an SNR of 20 dB from Fourier, Capon's, and MaxEnt methods are shown in the columns of the figure. The model structure includes the reflectivity of the aspect-sensitive scattering, which is centered at $(0.5^o, 0.5^o)$, and the transmitting beam pattern, which is directed vertically with a beam width of 3.6°. Notice the sidelobe effects in the Fourier brightness estimate for configuration 2, which has the longer baseline lengths.

for the case of configuration 2, where duplicate peaks are beginning to appear at the periphery of the image. Even for this configuration, Capon's and MaxEnt methods do not show such effects, which illustrates the sidelobe suppression capabilities of these two algorithms. As expected, the Fourier-based results for configuration 3 do not show the sidelobe patterns. However, the width of the brightness estimates is significantly overestimated because of the inherent resolution limitation. For this case of a broad brightness structure and SNR of 20 dB, MaxEnt qualitatively seems to provide the overall best performance.

Quantifying image quality is a difficult and ambiguous task. Typical quality measures are based on a function of the mean-squared error (MSE) or correlation [*Eskicioglu and Fisher*, 1995]. Several of-

ten used measures were calculated for this particular study. Although MSE can provide an overall measure of quality, it does not take into account slight shifts in peak location which would not be important for the interpretation of atmospheric data. In the present work, we have chosen to examine the capability of retrieving the characteristic structure of the model using the various algorithms and not slight shifts in angle. As a result, the peak of the normalized cross correlation between the model brightness and those estimated using the three techniques was used. The quality measure is defined in the following equation:

$$\max_{\Delta \mathbf{k}} \frac{\langle \mathbf{B}(\mathbf{k}, f)\hat{\mathbf{B}}(\mathbf{k}+\Delta\mathbf{k}, f)\rangle}{\sqrt{\langle \mathbf{B}(\mathbf{k}, f)^2\rangle \langle \hat{\mathbf{B}}(\mathbf{k}, f)^2\rangle}}, \tag{12}$$

where $\mathbf{B}(\mathbf{k}, f)$ and $\hat{\mathbf{B}}(\mathbf{k}, f)$ represent the model brightness distribution and estimated brightness distribution, respectively, and $\langle\ \rangle$ is the expected value operator. In this case, each brightness distribution image has 64×64 pixels and is normalized by its maximum value. The normalization was performed because it is desired to compare the statistical performance of the estimate of the overall structure of the image and not the accuracy of the absolute value of the brightness. By using the same data described in Figure 4 but with various values of SNR, quantitative comparisons among the Fourier-based, Capon's, and MaxEnt methods were made for the three antenna configurations. The calculated values of (12) are presented in Figure 5. For all SNR values (-5 to 20 dB), 50 trials were performed, each with an independent noise sequence added to the time series. Through averaging of the results of the 50 trials any deviation of the estimated brightness distribution caused by the random location of the simulated scattering points should not be significant. The mean of the 50 trials is shown in Figure 5. The standard deviation was calculated but proved to be exceedingly small compared to the mean and is therefore not shown. Configuration 1 should provide the least resolution per-

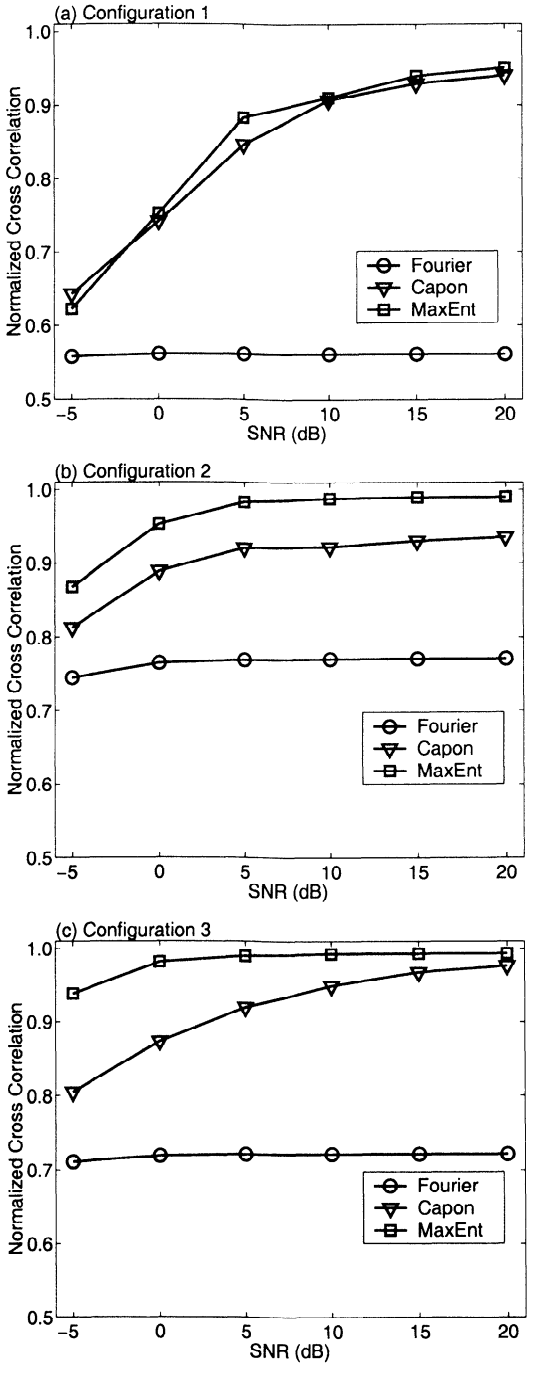

Figure 5. The maximum of the normalized cross correlation magnitude between the model and the estimated brightness from the three algorithms and for configurations (a) 1, (b) 2, and (c) 3 is shown. The correlation magnitude is shown as a function of SNR. The points on the curves represent the mean of 50 trials. As expected, configuration 3 produces the best results, with maximum correlation close to 1.0 for both the MaxEnt and Capon's methods. The resolution of the Fourier technique limits the maximum possible correlation to relatively low value.

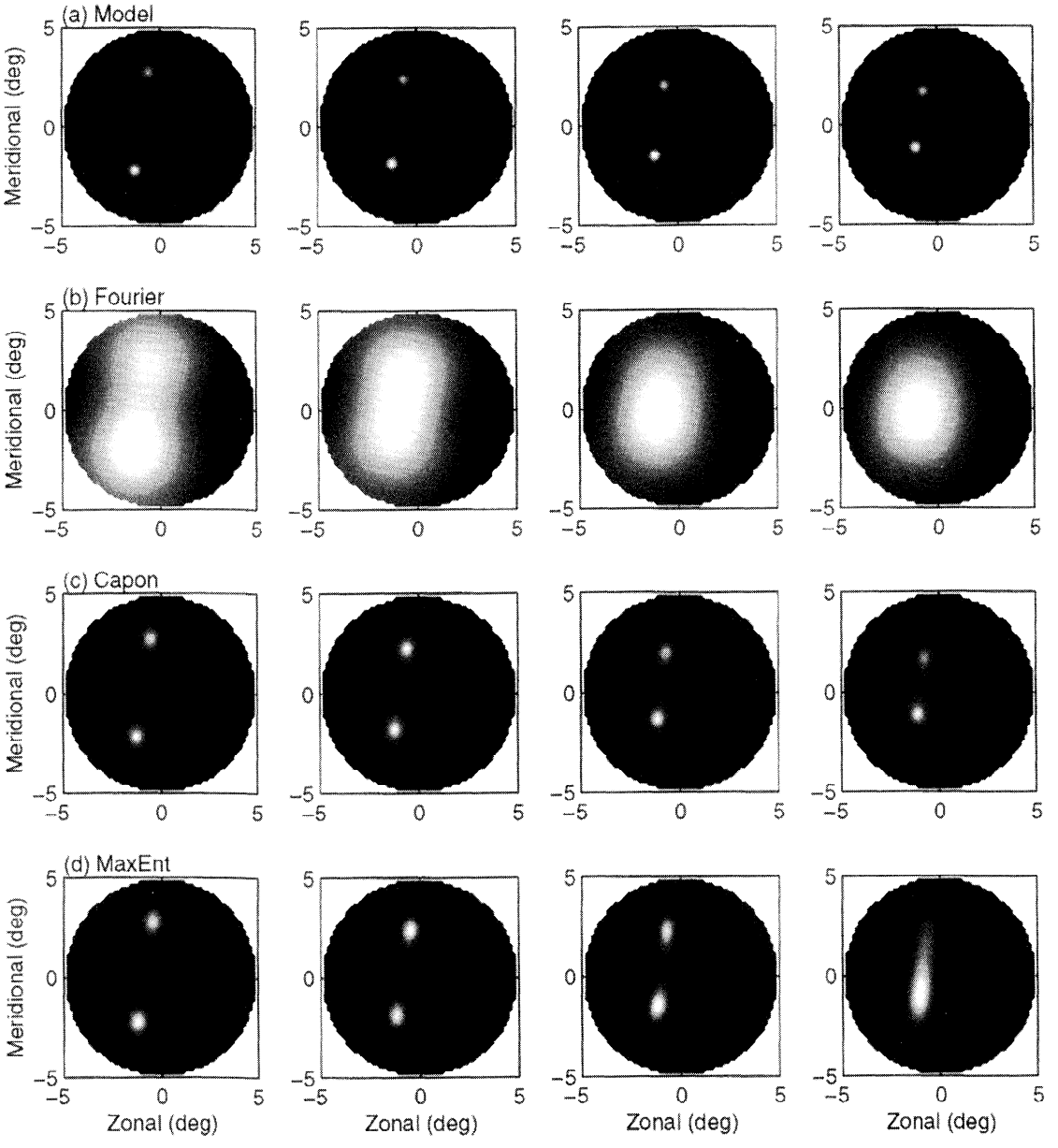

Figure 6. This localized scattering case attempts to elucidate the resolution limitations of the three methods. The model reflectivity is shown in Figure 6a for four different separations of the two scattering centers. As the points are placed closer together, the resolution of the algorithms will be tested. Estimated brightness distributions for an SNR of 20 dB and for the Fourier, Capon's, and MaxEnt methods are shown in Figure 6b, 6c, and 6d, respectively. Configuration 3 was used for all cases. Note the inability of the Fourier method to resolve the two peaks for all but the most separated case. Both the Capon's and MaxEnt methods are able to resolve the two peaks except in the closest case, where Capon's method exhibits slightly better qualitative performance.

formance since the baselines are relatively short. Notice that the results from this configuration exhibit the lowest correlation with a minimum of approximately 0.63 for the MaxEnt and Capon's methods for an SNR of -5 dB. MaxEnt and Capon's methods show extremely similar performance throughout the SNR range. The performance of the Fourier-based method is limited by the mainlobe width and sidelobe effects. As a result, an increase in SNR produces little noticeable change in performance.

Configuration 2 provides better quantitative results over configuration 1 for all methods with a distinct advantage becoming evident for the MaxEnt method. In fact, MaxEnt outperforms Capon's method for the entire range of SNR. In contrast, when configuration 3 is used, Capon's method begins to approach the performance of MaxEnt for the highest SNR values. For all cases, the Fourier-based method is inferior to the optimized methods.

3.3. Case 2: Localized Scattering Regions

Although the previous case is realistic for lower atmospheric turbulent scattering, it does not exercise the resolving capability of the CRI techniques. In order to study this characteristic a sequence of four independent brightness distributions was simulated, characterized by two narrow scattering regions. The separation of the scattering regions was decreased in order to test the resolution capabilities of the three algorithms. The four model brightness distributions are shown in Figure 6a. A total of 20 records of time series data were generated with the scattering region location updated every five records, which is equal to the number of incoherent integrations. The motion of the scattering regions is not related to the horizontal wind vector but could represent reflections from facets of an oscillating gravity wave, for example. Although not realistic, this case does provide a valuable test of resolution. Results from one realization of the simulation for an SNR of 20 dB are shown in Figure 6. Only configuration 3 results are shown in the figure. Both Capon's and MaxEnt methods are able to resolve the two peaks for larger separations. However, the smallest separation exemplifies the resolution limitation of the MaxEnt method where the algorithm does not resolve the two peaks. In contrast, Capon's method seems to exhibit two distinct peaks and may prove to possess higher resolution.

As was accomplished in the aspect-sensitive scattering case, the results from the two-scattering-region data are quantified through the calculation of the peak of the normalized cross correlation. For this case, the peak correlation value was averaged over the four different brightness distribution structures. Through this averaging process an overall quantitative measure of resolving power is obtained. As seen in the previous case, configuration 1 limits the performance of the algorithms as is shown in Figure 7. In fact, the results exhibit a quantitatively worse quality for all methods. It should be noted that the scale used in Figure 7 is different from that of Figure 5. Correlation values from configurations 2 and 3 are higher and begin to show an interesting SNR threshold, at approximately 10 dB, above which Capon's method outperforms the MaxEnt method. As expected, the Fourier-based method severely underperforms the other methods. It is also interesting that the accuracy of the estimated brightness distributions for all methods was superior for the aspect-sensitive scattering case. This fact illustrates the difficulty of observing the fine structure of the atmosphere.

4. Conclusions

CRI has recently been proposed as a method of probing the small-scale structure within the resolution volume of atmospheric radar systems. As such, the technique has the potential to reveal previously unobserved phenomena which occur on such small scales. The interpretation of the resulting brightness distribution becomes more important if a more complicated physical process exists within the resolution volume. For example, if there are multiple scattering centers moving with different velocities, then the estimates of angle of arrival and mean Doppler frequency will be biased using traditional algorithms. Many possible algorithms exist for the estimation of the so-called brightness distribution using sampled visibility data. The Fourier method is the most fundamental and is based on the inverse Fourier transform of the available visibility data. As a result, well-known resolution limitations exist biasing the results. Two more sophisticated algorithms, MaxEnt and Capon's methods, have recently been applied to the atmospheric radar case. However, no statistical verification has been presented in the literature to date. The present work has detailed a simulation study of the three CRI techniques. A mathematical summary of the Fourier-based, Capon's, and MaxEnt methods was presented in section 2. Capon's method

takes advantage of the information provided from the data by adaptively adjusting the manner in which the signals are combined. The MaxEnt method uses an optimized model of the brightness distribution to avoid the biases caused by sampling of the visibility function.

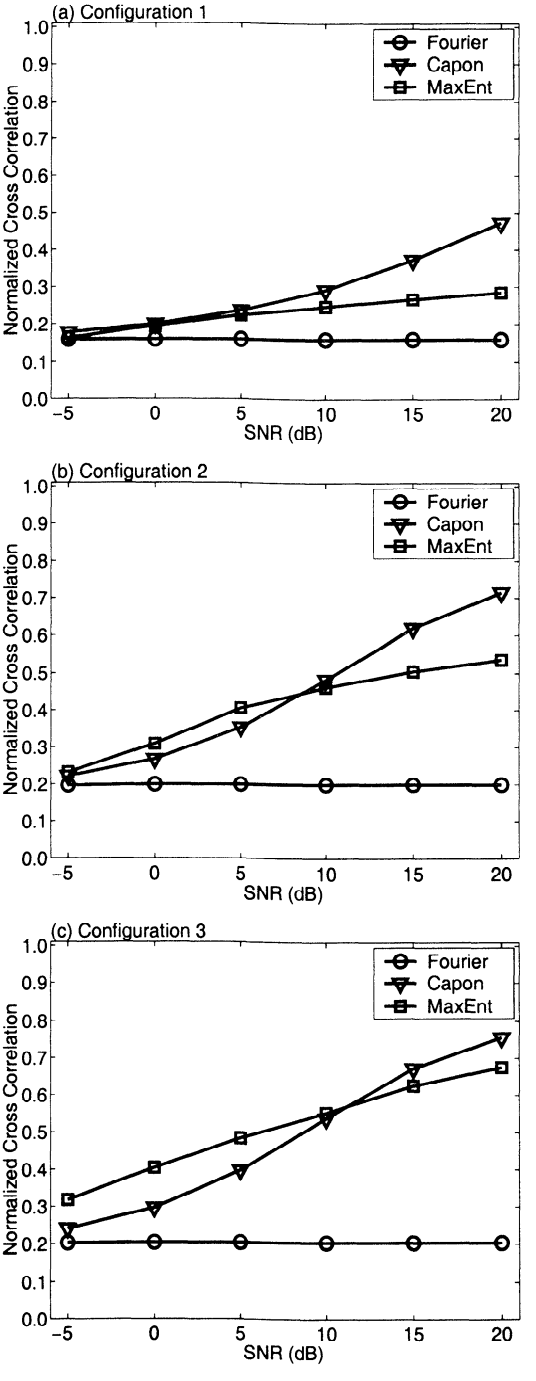

Performance of the three CRI techniques was tested for a VHF wavelength at an altitude of 10 km. It is expected that these results apply to other height regions as well. The effects of antenna configuration and SNR were quantified through the calculation of the maximum of the normalized cross correlation between the estimated brightness and the known model. As expected, the results showed the inherent limitations of Fourier-based CRI. Angular aliasing effects were evident for this method for configuration 2, in particular, which possessed the most severe grating lobe problem. In the case of aspect-sensitive scattering the MaxEnt method outperformed the other two methods in all cases with correlation values close to unity. In order to study fine-scale structure, high angular resolution is needed. Therefore a second test case was generated, characterized by two localized scattering regions. By varying the spacing between the regions the resolution limitations could be examined. The results suggest that Capon's method possesses superior resolution capabilities for high SNR. In contrast, the MaxEnt method outperformed all methods for low SNR. For this particular case the SNR threshold was approximately 10 dB.

Although comparisons of the absolute power density and Doppler frequency estimates using the three CRI techniques are not our main concern, it is thought that the Fourier method would provide the most robust power density estimate among these techniques with the caveat of the well-known resolution limitations. However, the high-resolution techniques are expected to obtain a better frequency estimate when there exist multiple distinct scattering regions, since the Doppler frequency estimate is a weighted volume average in the resolution volume. The Fourier method produces a wider beam width and therefore more bias in the frequency estimate.

Figure 7. This figure is similar to Figure 5 except that the maximum correlation values were calculated as an average of the sequence of four images shown in Figure 6. Therefore the values can be used to represent the overall quality of the brightness estimates for the localized scattering case. Again, the results are given for configurations (a) 1, (b) 2, and (c) 3. The results indicate that a threshold exists at an approximate SNR of 10 dB, below which MaxEnt has superior performance. However, results with SNR above 10 dB show a larger correlation for Capon's method.

Another interesting point of comparison would be the determination of the aperture needed to produce equivalent resolution for the three methods. Unfortunately, this comparison cannot be made in general since both Capon's and MaxEnt methods are dependent on the specific data. For example, if a constant brightness distribution exists, the array characteristic could be quantified and the equivalent receiver configuration could be determined. However, the results would not hold for all situations because of the adaptive characteristic of both the Capon and MaxEnt methods.

When making the choice between the various algorithms available for image reconstruction, one must take into account the computational complexity of the methods. The MaxEnt method is based on the optimization of a set of highly nonlinear equations, must be performed iteratively, and is therefore extremely computationally intensive. In contrast, Capon's method simply involves the inversion of an $n \times n$ matrix as shown in (5). Therefore constraints of the particular application will ultimately dictate the algorithm of choice. More accurate estimates of the brightness distribution, from an information theory point of view, are possible with the MaxEnt method. However, Capon's method can produce comparable results and, in some high-SNR cases, can even outperform the MaxEnt technique.

Acknowledgments. R.D.P. and T.-Y.Y. were supported by the Division of Atmospheric Sciences of the National Science Foundation through grant ATM 99-08616. D.L.H. was supported by the Division of Atmospheric Sciences of the National Science Foundation through grant ATM 97-11236. The authors would like to thank D. A. Holdsworth for his useful discussions of the simulation procedure and S. Surendran for his comments on the original manuscript.

References

Capon, J., High-resolution frequency-wavenumber spectrum analysis, *Proc. IEEE*, *57*, 1408–1419, 1969.

Eskicioglu, A. M., and P. S. Fisher, Image quaity measurement and their performance, *IEEE Trans. Commun.*, *43*, 2959–2965, 1995.

Fukao, S., T. Sato, S. Kato, R. M. Harper, R. F. Woodman, and W. E. Gordon, Mesospheric winds and waves over Jicamarca on May 23-24, 1974, *J. Geophys. Res.*, *84*, 4379–4386, 1979.

Gage, K. S., and J. L. Green, Evidence for specular reflection from monostatic VHF radar observations of the stratosphere, *Radio Sci.*, *13*, 991–1001, 1978.

Gull, S. F., and G. J. Daniell, Image reconstruction from incomplete and noisy data, *Nature*, *272*, 686–690, 1978.

Holdsworth, D. A., Signal analysis with applications to atmospheric radars, Ph.D. thesis, Univ. of Adelaide, Adelaide, south Aust. Austrialia, 1995.

Holdsworth, D. A., and I. M. Reid, A simple model of atmospheric radar backscatter: Description and application to the full correlation analysis of spaced antenna data, *Radio Sci.*, *30*, 1263–1280, 1995.

Hysell, D. L., Radar imaging of equatorial *F* region irregularities with maximum entropy interferometry, *Radio Sci.*, *31*, 1567–1578, 1996.

Hysell, D. L., and R. F. Woodman, Imaging coherent backscatter radar observations of topside equatorial spread *F*, *Radio Sci.*, *32*, 2309–2320, 1997.

Kudeki, E., and F. Sürücü, Radar interferometric imaging of field-aligned plasma irregularities in the equatorial electrojet, *Geophys. Res. Lett.*, *18*, 41–44, 1991.

Palmer, R. D., S. Gopalam, T. Yu, and S. Fukao, Coherent radar imaging using Capon's method, *Radio Sci.*, *33*, 1585–1598, 1998a.

Palmer, R. D., M. F. Larsen, S. Fukao, and M. Yamamoto, On the relationship between aspect sensitivity and spatial interferometric in-beam incidence angles, *J. Atmos. Sol.-Terr. Phys.*, *60*, 37–48, 1998b.

Röttger, J., and C. H. Liu, Partial reflection and scattering of VHF radar signals from the clear atmosphere, *Geophys. Res. Lett.*, *5*, 357–360, 1978.

Shannon, C. E., and W. Weaver, *The Mathematical Theory of Communication*, Univ. of Ill. Press, Urbana, 1949.

Thompson, A. R., *Interferometry and Synthesis in Radio Astronomy*, John Wiley, New York, 1986.

Woodman, R. F., Inclination of the geomagnetic field measured by an incoherent scatter technique, *J. Geophys. Res.*, *76*, 178–184, 1971.

Woodman, R. F., Coherent radar imaging: Signal processing and statistical properties, *Radio Sci.*, *32*, 2372–2391, 1997.

D. L. Hysell, Department of Physics and Astronomy, Clemson University, Clemson, SC 29634-1911. (dhysell@clemson.edu)

R. D. Palmer and T.-Y. Yu, Department of Electrical Engineering, University of Nebraska, Lincoln, NE 68588-0511. (rpalmer2@unl.edu; tian@doppler.unl.edu)

(Received July 30, 1999; revised March 3, 2000; accepted May 31, 2000.)